BIOCHEMISTRY
including biophysical chemistry & molecular biology

Article

pubs.acs.org/biochemistry

Nonspecific Prion Protein–Nucleic Acid Interactions Lead to Different Aggregates and Cytotoxic Species

Bruno Macedo,[†] Thiago A. Millen,[‡] Carolina A. C. A. Braga,[‡] Mariana P. B. Gomes,[†] Priscila S. Ferreira,[‡] Julia Kraineva,[§] Roland Winter,[§] Jerson L. Silva,[‡] and Yraima Cordeiro*,[†]

[†]Faculdade de Farmacia, Universidade Federal do Rio de Janeiro, RJ 21941-590, Rio de Janeiro, Brazil

[‡]Instituto de Bioquimica Medica, Universidade Federal do Rio de Janeiro, Rio de Janeiro, Brazil

[§]Faculty of Chemistry, Physical Chemistry I, Dortmund University, Dortmund, Germany

Supporting Information

ABSTRACT: A misfolded form of the prion protein (PrP) is the primary culprit in mammalian prion diseases. It has been shown that nucleic acids catalyze the misfolding of cellular PrP into a scrapie-like conformer. It has also been observed that the interaction of PrP with nucleic acids is nonspecific and that the complex can be toxic to cultured cells. No direct correlation has yet been drawn between changes in PrP structure and toxicity due to nucleic acid binding. Here we asked whether different aggregation, stability, and toxicity effects are detected when nonrelated DNA sequences interact with recombinant PrP. Using spectroscopic techniques to analyze PrP tertiary and secondary structure and cellular assays to assess toxicity, we found that rPrP–DNA interactions lead to different aggregated species, depending on the sequence and size of the oligonucleotide tested. A 21-mer DNA sequence (D67) induced higher levels of aggregation and also dissimilar structural changes in rPrP, compared to binding to oligonucleotides with the same length and different nucleotide sequences or different GC contents. The rPrP–D67 complex induced significant cell dysfunction, which appears to be correlated with the biophysical properties of the complex. Although sequence specificity is not apparent for PrP–nucleic acid interactions, we believe that particular nucleic acid patterns, possibly related to GC content, oligonucleotide length, and structure, govern PrP recognition. Understanding the structural and cellular effects observed for PrP–nucleic acid complexes may shed light on the still mysterious pathology of the prion protein.

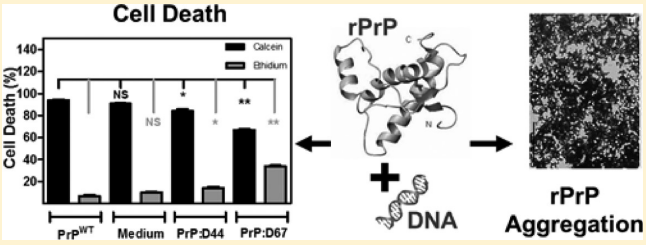

Prion diseases or transmissible spongiform encephalopathies (TSEs) are neurodegenerative disorders that affect humans and other animals.[1] There is no current therapy for these diseases, and the molecular mechanisms that lead to TSE development are still under investigation.

TSEs are triggered by the conversion of the cellular prion protein (PrP^{C})[1,2] into a pathological conformer, the scrapie PrP (PrP^{Sc}), which has a higher β-sheet content.[3,4] This conversion is promoted by PrP^{Sc}.[5,6] Although there are reports indicating that recombinant PrP alone can aggregate, be toxic to cells,[7] and cause a prion-like disease in animals,[8] other evidence indicates that this process can also be modulated by additional macromolecules.[9−13] Among these other molecules, nucleic acids (NAs) are believed to act as catalysts in this process (reviewed in refs 14 and 15). Aberrant interactions between proteins and nucleic acids have been implicated in other neurodegenerative diseases,[16,17] as well. On the other hand, synthetic modified oligonucleotides have been shown to reverse prion infectivity both in cell-based assays and in prion animal models.[18,19]

The interaction of prion protein (PrP) with nucleic acids has been shown to occur both ex vivo and in vitro.[11,20,21] The reaction product, the PrP–NA complex, is sometimes proteinase K-resistant and undergoes amyloid oligomerization.[21−23] Depending on the binding conditions, this interaction can also convert PrP into an aggregated β-sheet-rich structure.[11] In previous studies, we found indications that host nucleic acids catalyze the conversion between PrP^{C} and PrP^{Sc} by reducing the protein's mobility and by favoring protein–protein interactions.[11,15] In addition, PrP^{C} has been found to localize to the nucleus of neuronal and endocrine cells and to interact with chromatin components.[24]

Recent studies indicate that the minimal components required for the in vitro conversion of PrP^{C} into PrP^{Sc} are polyanions, mainly RNA molecules and lipids.[25,26]

Despite recent reports (for reviews, see refs 14 and 15) describing the effects of nucleic acids on PrP conversion, the question of whether nucleic acids are indeed involved in triggering prion diseases is still under debate. Our limited understanding of this subject may be explained by the lack of structural and pathophysiological data for the PrP–NA complex.

Received: October 10, 2011
Revised: June 9, 2012
Published: June 12, 2012

Depending on the system and oligonucleotide used, nucleic acid sequences can also inhibit prion protein aggregation, which was shown when an aggregation-prone hydrophobic prion protein domain was incubated with different oligonucleotide sequences.[11] Moreover, modified NAs might also be useful for the treatment and diagnosis of prion diseases. It has been shown that phosphorothioate oligonucleotides bind to PrP, can reduce the level of accumulation of PrP^{Sc} in scrapie-infected cell lines,[18,19,27] and can preferentially bind to PrP^{C} or PrP^{Sc}.[28] These studies indicate a dual role for nucleic acids in prion aggregation.

It has been observed that the interaction of PrP with nucleic acids is nonspecific because this protein binds several different RNA and DNA sequences in vitro.[11,22,28,29] The PrP−NA complex can also be toxic to cultured cells.[22,30] Knowing whether this effect is associated with specific nucleic acid sequences and/or structures would be enlightening. To answer this essential question, we started by asking whether different aggregation, stability, and toxicity effects are detected when different DNA sequences are tested. Using spectroscopic techniques to analyze PrP tertiary and secondary structure and cellular assays to check for toxicity, we found that a given nucleic acid sequence might be associated with a particular effect.

EXPERIMENTAL PROCEDURES

Construction, Expression, and Purification of Recombinant Prion Proteins. Heterologous expression in *Escherichia coli* and the further purification and oxidative refolding of the recombinant prion proteins rPrP23−231 and rPrPΔ51−90 followed the same previously described protocol.[11,31]

Reagents and Protein Sample. All reagents used were of an analytical grade. D_2O (deuterium oxide) for Fourier transform infrared spectroscopy (FTIR) was purchased from Aldrich (Seelze, Germany). Unless otherwise stated, measurements were always performed in 10 mM (pH 7.4) Tris buffer supplemented with 100 mM NaCl. FTIR spectroscopy was performed in Tris buffer (pH 6.5) supplemented with 100 mM NaCl for temperature-dependent measurements. All samples for FTIR spectroscopy were lyophilized three times to remove all H_2O and then diluted to 4% (w/w) in 99.9% D_2O. Synthetic, single-stranded sequences 5′-GTA ACC GAA ATC GGT TGA-3′ (D44) and 5′-AAA GGA CGC GCG CGC GCG TTA-3′ (D67) were purchased from Integrated DNA Technologies (Coralville, IA). Other sequences derived from the original D44 and D67 oligonucleotides were also acquired from IDT: 5′-GTG GCC GGG GTC GGT TGG-3′ (D44G) (all A residues in D44 were substituted with G residues), 5′-AAA AAA CAC ACA CAC ACA TTA-3′ (D67A) (all G residues in D67 were substituted with A residues), 5′-AGT GTT AGG TAG CAC AAC-3′ (D44s) (a scrambled version of D44), and 5′-GCG TCG GCG GAT ACG AAC CAG-3′ (D67s) (a scrambled version of D67). The D44s and D67s sequences were generated using a software tool to create scrambled sequences as negative controls (https://www.genscript.com/ssl-bin/app/scramble). Full hybridization of DNA sequences and double-stranded oligo concentrations was assessed as previously described.[32] We also ordered a ribonucleotide identical to D67: 5′-AAA GGA CGC GCG CGC GCG UUA-3′ (R67). The Syrian hamster PrP peptide (residues 109−149) was acquired from Genemed Synthesis, Inc. (San Antonio, TX), synthesized in solid phase, and purified by reverse phase high-performance liquid chromatography (>90% purity). The peptide was solubilized just before use in 50 mM MES (4-morpholinoethanesulfonic acid) buffer (pH 5.0) supplemented with 6 M urea and 10 mM sodium dodecyl sulfate (SDS). Peptide aggregation was performed as previously described.[33] The sequence of the prion peptide used was 109-MKHMAGAAAAGAVVGGLGGWMLGSAMSRPMMH FGNDWEDRY-149.

Spectroscopy. Light scattering (LS) and fluorescence spectra were recorded using an ISSPC1 (ISS, Champaign, IL) or a Jasco FP6300 spectrofluorimeter (Jasco Corp., Tokyo, Japan). LS was measured at 90 °C by illuminating the samples at 320 nm and collecting LS from 300 to 340 nm. The tryptophan fluorescence of rPrP23−231 was measured by exciting the samples at 280 nm and detecting the emission at 300−420 nm. For the Stern−Volmer plot, the constant (K_{sv}) was obtained after linear regression of the F_0/F versus acrylamide concentration curve, where F_0 is the initial fluorescence intensity, F is the fluorescence intensity at the specified acrylamide concentration, and $F_0/F = 1 + K_{sv}[Q]$.

Fourier Transform Infrared (FTIR) Spectroscopy. The FTIR spectra were recorded with a Nicolet 6700 spectrometer (Thermo Scientific) equipped with a MCT-B detector operated at −196 °C. Each spectrum was obtained by collecting 256 scans at a spectral resolution of 2 cm^{-1} and was apodized with a Happ−Genzel function. The buffer or DNA spectrum was considered the background signal. The spectrometer chamber was purged with dry and carbon dioxide-free air. For the temperature-dependent experiments, sample chambers with 4 mm thick CaF_2 windows and an optical path length of 50 μm were used. An external thermostat was used to maintain the temperature within 0.1 °C. Samples were maintained at each temperature for 15 min to reach stabilization. Fourier self-deconvolution of the FTIR spectra was performed with a resolution enhancement factor of 1.8 and a bandwidth of 15 cm^{-1}. Peak position and curve fitting were determined using OMNIC (Nicolet, WI) and GRAMS (Galactic), respectively. The integral intensities of the secondary structure elements of rPrP were calculated by analysis of the amide I′ vibration mode of the infrared spectrum.[34,35] The amide I′ mode of rPrP was fit in the range between 1695 and 1596 cm^{-1} and analyzed using six mixed Gaussian−Lorentzian functions.[31,35] From the parameters found, the peak areas (integral intensities) of all components were calculated. For the DNA binding data, spectra of free DNA were utilized as a baseline for the respective rPrP−DNA complex spectrum. The medium temperature of the transition ($T_{1/2}$) was calculated from a sigmoidal equation fit to the β-sheet content changes upon heating of the samples.

Far-UV Circular Dichroism. Circular dichroism (CD) spectra were recorded with a Chirascan spectropolarimeter (Applied Photophysics, Surrey, U.K.) at 25 °C with 2.00 mm path length quartz cells. The buffer spectrum was subtracted for all spectra. Four scans were collected per experiment, and each experiment was performed in triplicate.

Transmission Electron Microscopy (TEM). Samples were adhered to a carbon-coated grid, blotted to remove extra material, and stained for 60 s with a 2% solution of uranyl acetate prepared in water. Images were digitally collected with a Jeol 1200 electron microscope operating at 80 kV.

Murine Neuroblastoma Cell (N2a) Culture and Cell Viability Assays. N2a cells were grown in 75 cm^2 flasks in DMEM (Dulbecco's modified Eagle's medium) supplemented

with 10% FBS (fetal bovine serum), 1 mM HEPES buffer, 2 mM L-glutamine, and 100 μg/mL gentamicin (complete cell media) and incubated at 37 °C in a 5% CO_2 atmosphere. Adhered cells were replated every 2−3 days after trypsin treatment and dilution at a 1:4 to 1:6 ratio with complete cell media. For the viability assay, N2a cells (2−3-day-old cultures of up to 80% confluence) were plated into 96- or 24-well plates, depending on the assay, in complete cell media at a density of ∼5000 cells/well, and incubated overnight at 37 °C in a 5% CO_2 atmosphere. The media from the cultured cells were then removed, and 100 or 400 μL of the samples containing free rPrP23−231, free DNA, and rPrP−DNA complexes was immediately added to each well. All the samples were filter-sterilized, and appropriate dilutions were prepared in complete cell media. At least six wells containing cells and six wells without cells received 100 μL of medium only to serve as controls and blanks, respectively. After 72 h, the cytotoxicity assays were performed.

The MTT [3-(4,5-dimethylthiazol-2-yl)-2,5-diphenyltetrazolium bromide] reduction assay was performed as follows. Twenty-five microliters per well of MTT (5 mg/mL in PBS) was added to the wells (samples, blanks, and controls), and the plates were incubated for 3−4 h at 37 °C. All the medium with MTT was carefully removed, and 150 μL of DMSO was added to each well to solubilize the formazan produced, which was quantified by reading the OD at 570 nm in a 96-well plate reader (Spectramax M5, Molecular Devices). Mean values and standard deviations were calculated from triplicates of independent experiments.

LIVE/DEAD assays (LIVE/DEAD Viability/Cytotoxicity kit for mammalian cells, Invitrogen Corp.) were performed in 24-well plates, as previously described.[22] LIVE/DEAD images were acquired using a Zeiss Observer.Z1 microscope (serial number 3834000373, Carl Zeiss Inc.). The Hoechst 33342 probe (Molecular Probes Inc., Eugene, OR) was also utilized to evaluate cellular survival. All the assays were performed in triplicate. A Viability/Cytotoxicity Assay kit for Animal Live & Dead Cells was also used in a 96-well plate, following the protocol provided by the company (Biotium Inc.). Briefly, 5000 cells were transferred to each well, and after 24 h, the samples (as described above) were applied and incubated for 72 h at 37 °C in a 5% CO_2 atmosphere. Culture medium (DMEM) was removed, and the kit reagents were added to each well and incubated for 40 min. The assay was read by following calcein (excitation at 485 nm, emission at 530 nm) and ethidium (excitation at 530 nm, emission at 645 nm) fluorescence in a plate spectrofluorimeter (Spectramax M5, Molecular Devices).

Statistics. Statistical analyses were performed using Sigma Plot (version 10.0) or GraphPad Prism. For the cellular viability assays, we used a one-way ANOVA Tukey test to determine which differences were significant between the control (buffer) and the results that were obtained in the presence of free rPrP, oligonucleotides, and the rPrP−DNA complexes (*P < 0.05, **P < 0.01, and ***P < 0.001). Unless otherwise specified, all data shown are the mean of triplicates, and the error bars indicate the standard error (SEM) or are representative of at least two independent experiments.

RESULTS

DNA-Dependent Secondary and Tertiary Structural Changes in rPrP. We investigated whether two previously identified DNA sequences differently affect the aggregation and structure of rPrP. We selected the double-stranded DNA sequence D44 that was characterized by our group as a high-affinity rPrP ligand.[11,36,37] The second oligonucleotide, D67, which also binds rPrP (unpublished data), was modified from a 34 bp polyGC sequence[11] and contains a 12-base GC core. As control sequences (constructed from the original D44 and D67), we used D44G (all A residues in D44 were substituted with G residues), D67A (all G residues in D67 were substituted with A residues), two scrambled versions of D44 and D67, D44s and D67s, respectively, and a ribonucleotide sequence related to D67, R67 (see Experimental Procedures for details).

We observed the rPrP fluorescence emission and light scattering in the presence of D67 and D44 (Figure 1). An

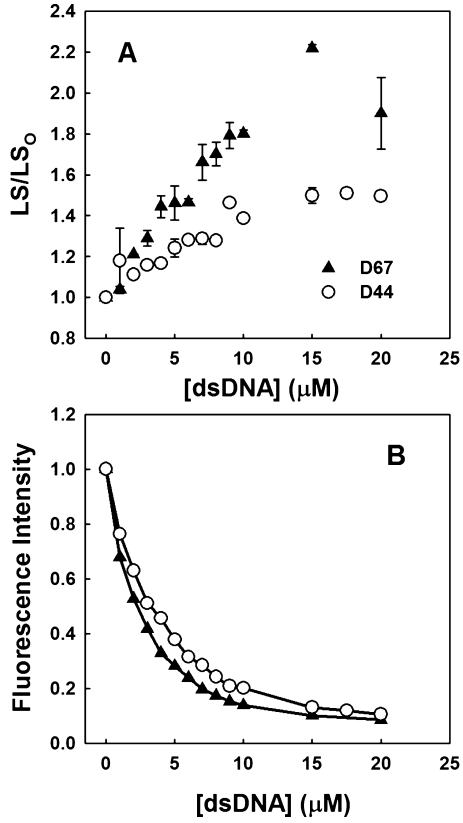

Figure 1. DNA binding induces rPrP oligomerization and suppresses intrinsic fluorescence emission. Relative light scattering (LS) intensity (A) and the normalized fluorescence area (B) of rPrP23−231 (2.5 μM) titered with D67 or D44. For the LS measures, samples were illuminated at 320 nm and the LS values were collected from 300 to 340 nm. In panel B, the excitation was set at 280 nm and the emission was recorded from 300 to 420 nm.

increase in LS was observed (Figure 1A), suggesting that rPrP oligomerizes after DNA addition. The binding of both DNA oligos to rPrP suppressed tryptophan fluorescence emission (Figure 1B), indicating that the tryptophan environment is modified upon oligonucleotide interaction. rPrP tertiary structure changes mediated by the other oligonucleotides were also investigated (Figure S1 of the Supporting Information). There was no significant difference between those sequences, all quenched tryptophan fluorescence, and induced protein oligomerization (Figure S1 of the Supporting Information); however, the longer (21-mer) sequences (D67A and D67s) induced higher LS values than the D44 sequences (Figure S1 of the Supporting Information). Interaction of rPrP with the R67 ribonucleotide resulted in higher LS values, as

expected.[22] However, it is not possible to directly compare the effects of the D67 and R67 sequences because the structures of RNA and DNA oligonucleotides are different and the interaction of rPrP with RNA involves rPrP regions other than those interacting with DNA.[22,36]

Interestingly, addition of the D44 and D67 oligos to rPrP at a protein:DNA molar ratio of 1:1 or even 2:1 led to prompt aggregation (Figure S2 of the Supporting Information). However, this process was partially reversible because both LS and the center of spectral mass values returned to values close to that of the free rPrP approximately 1 h later (Figure S2 of the Supporting Information). Note that for D67 binding, the LS values remained higher than that for the rPrP−D44 complex, even after incubation with rPrP for 1 h (Figure S2 of the Supporting Information). The differences related to the slow addition of oligonucleotides to rPrP most likely occur because when added, small quantities of DNA are incorporated into rPrP, even though they do not lead to aggregation.

We also analyzed the interaction between DNA and the rPrPΔ51−90 mutant. This mutant does not possess amino acid residues 51−90, i.e., the PrP octarepeat region.[31] Although rPrPΔ51−90 binds DNA, we observed no significant increase in LS upon titration of DNA into the protein sample (Figure S3 of the Supporting Information).

Secondary structural changes were monitored by CD and FTIR. We observed that the rPrP α-helical content (observed at 222 nm) decreased when the protein bound to either the DNA sequence, D44, or D67 (Figure 2). Similar secondary structure

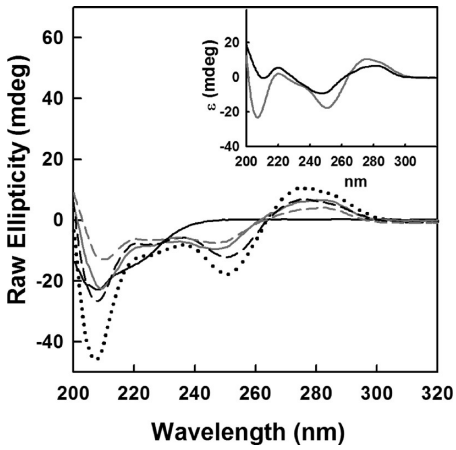

Figure 2. Changes in the secondary structure content of rPrP23−231 upon DNA binding, as revealed by circular dichroism (CD) spectroscopy. CD spectra of free rPrP23−231 at 10 μM (solid black line), the 1:1 rPrP−D44 complex (dashed gray line), the 1:1 rPrP−D67 complex (dashed black line), and the sum of the individual components rPrP and D44 (solid gray line) or D67 (dotted black line). The inset shows the CD spectra of free D44 (black) and D67 (gray) at 10 μM. The spectra were collected immediately after the addition of DNA to the sample.

changes were observed when rPrP interacted with a 28-mer DNA.[11] Analysis of the DNA CD signals indicated that the ellipticity values at ∼250 nm (base stacking) and 275 nm (right-handed helicity) did not change significantly. However, we observed a decrease in the intensity of the bands upon rPrP binding (Figure 2), indicating that rPrP binds the DNA grooves.[38] An increase in β-sheet secondary structure content was not visible in these spectra because the CD spectra of the unbound DNA oligos were not subtracted. We then compared the sum of the spectra of free DNA and rPrP (Figure 2, dotted black line for D67) with the spectrum of the complex (rPrP−D67) (Figure 2, dashed black line). We observed a change in the rPrP structure while in the presence of DNA. This change cannot be attributed to the presence of the DNA signal only. After binding equilibrium was reached (after incubation with DNA for 48−72h), we observed that part of the native secondary structure of either the protein or the nucleic acid was recovered (Figure S4 of the Supporting Information). This recovery was greater for the rPrP−D44 complex, and interaction of rPrP with the control oligonucleotides (D44G, D44s, D67A, and D67s) resulted in similar structural changes, with a loss of protein secondary structure even after binding equilibrium had been reached (Figure S5 of the Supporting Information).

The impact of the double-stranded DNA binding on the secondary structure of full-length rPrP23−231 and rPrPΔ51−90 was compared by FTIR spectroscopy (Table 1 and Figure S6 of the Supporting Information).

The amide I′ region of free rPrP23−231 and free rPrPΔ51−90 or of the DNA-bound forms was analyzed. We incubated the rPrP constructs with D44 or D67 for 3 days to reach binding equilibrium (disaggregation). Six bands in the second-derivative spectra were found to contribute to the overall amide I′ area, and the peak positions and areas relative to the total area of the amide I′ region are listed in Table 1. The addition of DNA to rPrP23−231 induced slight conformational changes in the protein's secondary structure (Table 1). Full-length rPrP incubated with D44 at a 1:1 molar ratio led to an increase in the content of β-sheet structure (∼4%) and also in turns (∼7%), with a loss of random structure [∼10% (Table 1)]. For D67 binding, we observed a significant increase in turn content and a loss of random conformations only, with a decrease in random coil structure content of ∼7% and an increase in turn content of ∼6%. For the rPrPΔ51−90 mutant, we observed no significant structural changes upon binding to both D44 and D67 (Figure S6 of the Supporting Information).

Fluorescence quenching by acrylamide revealed different tertiary structure changes upon DNA binding by rPrP (Figure 3). We observed that Trp residues are protected from the solvent in the presence of the oligonucleotides, indicating that rPrP presents a smaller accessible surface area when bound to DNA, which might reflect the oligomerization process. There are significant differences between the Stern−Volmer constants (K_{sv}) for rPrP bound to D67 and bound to D44 (Table S2 of the Supporting Information). This difference indicates that the tryptophan residues are more protected when rPrP interacts with the D67A and D67s sequences than with all D44 sequences, supporting the notion that the size of the oligonucleotide dictates aggregation propensity, which is reflected in the protection of tryptophan residues from the quencher. However, it is important to note that the D44 sequences presented a similar protection profile while the D67 sequences differed among each other, with D67 leading to less protection of Trp residues than D67A and D67s (Figure 3). This observation might reveal subtle differences between those sequences, which are not related to size or GC content. The rPrP−D67 complex probably adopts a particular conformation, which could be revealed only by high-resolution techniques that would yield the three-dimensional structure of the complex.

Different Stabilities of Soluble rPrP−DNA Complexes. It has previously been observed that the binding of D44 to murine rPrP increases its protein stability against urea and

dx.doi.org/10.1021/bi300440e | Biochemistry 2012, 51, 5402−5413

Table 1. FTIR Analysis of the Secondary Structure Content of Free and DNA-Bound rPrP23−231[a]

	rPrP23−231, native		rPrP23−231 with D44		rPrP23−231 with D67	
Structural assignment	Wavenumber (cm^{-1})	Area (%)	Wavenumber (cm^{-1})	Area (%)	Wavenumber (cm^{-1})	Area (%)
β-sheets	1680, 1627, 1613	14.7	1677, 1630, 1612	18.0	1679, 1627, 1613	14.5
turns	1669	11.3	1668	18.1	1668	17.6
α-helix	1652	25.5	1653	26.7	1653	26.2
random coil	1642	48.4	1642	37.2	1641	41.7

[a]FTIR spectra were recorded at 25 °C. The estimated error in the wavenumbers is ±1 cm^{-1} and ±2% for the peak areas. Data for free rPrP23−231 are shown as previously described.[35]

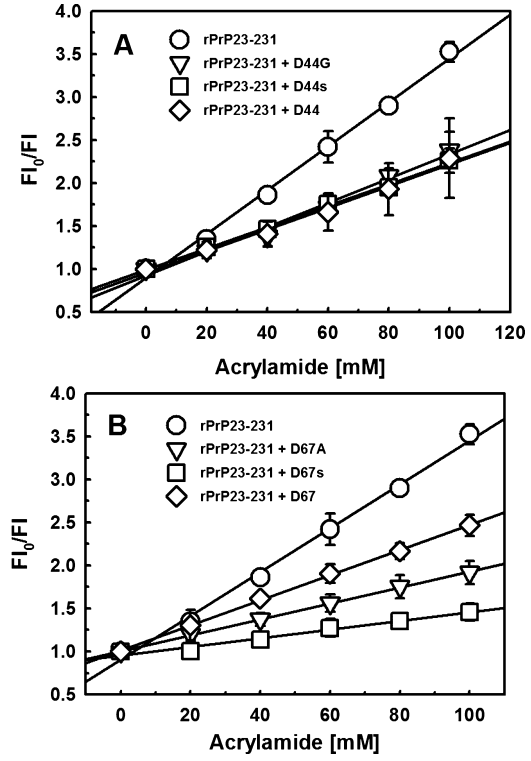

Figure 3. Collisional quenching by acrylamide. The decrease in intensity is described by the ratio of the fluorescence in the absence of quenching to that in the presence of quencher by the Stern−Volmer equation. rPrP23−231 free or bound to DNA was used at 2.5 μM (protein:DNA molar ratio of 1:1): (A) (○) rPrP23−231, (▽) rPrP23−231 with D44G, (□) rPrP23−231 with D44s, and (◇) rPrP23−231 with D44 and (B) (○) rPrP23−231, (▽) rPrP23−231 with D67A, (□) rPrP23−231 with D67s, and (◇) rPrP23−231 with D67. Error bars represent the average values of three independent measurements.

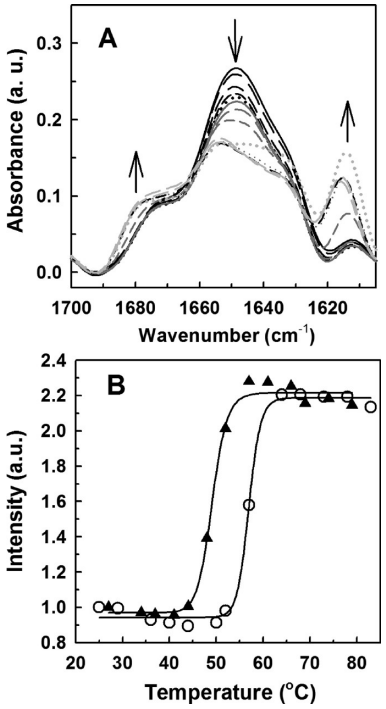

Figure 4. DNA-induced rPrP23−231 thermal stability. rPrP23−231 incubated with D44 was submitted to a temperature increase up to 80 °C. FTIR spectra were collected at each 5 °C increment. (A) Spectra of the rPrP−D44 complex were subtracted from their respective DNA background spectrum. Only selected temperatures are shown (arrows indicate changes with an increase in temperature). (B) Changes in β-sheets of the rPrP−D44 (○) or rPrP−D67 (▲) complex. All FITR data were collected after incubation of the rPrP−DNA complex at a 2:1 molar ratio for 3 days.

guanidine hydrochloride denaturation, which is also enhanced at lower pHs.[37] We used FTIR spectroscopy to evaluate whether DNA binding would provide increased thermal stability for rPrP (Figure 4). We performed thermal denaturation curves for rPrP in the presence and absence of D44 (Figure 4A) and D67 sequences and analyzed the protein secondary structural changes with an increase in temperature. We evaluated the rPrP−DNA complexes in the nonaggregated state after incubation with DNA for 3 days. The infrared signals of the free oligonucleotides were collected as well. These data revealed that, because of the low signal intensity, the protein amide I′ band region was not significantly disturbed by the DNA signal (data not shown). We could observe that the rPrP−D44 complex aggregated at higher temperatures than the rPrP−D67 complex by following the β-sheet content of the protein with an increase in temperature (Figure 4B).

Both rPrP−DNA complexes presented similar unfolding behavior. However, the temperature-induced aggregation could be distinguished for both DNA sequences. Full-length rPrP is stabilized in the presence of D44. The $T_{1/2}$ for aggregation was 56.9 ± 1.2 °C, in comparison to the D67 complex, for which a $T_{1/2}$ value of 49.1 ± 0.3 °C was observed (calculated from the plots in Figure 4B). Free rPrP23−231 presented a $T_{1/2}$ of 45.3 ± 1.9 °C. In contrast, binding of rPrPΔ51−90 to both DNA sequences led to a slight destabilization of the protein, and no significant changes in secondary structure were observed (Figure S6 of the Supporting Information).

Binding of rPrP to Double-Stranded DNA Leads to the Formation of Fractal-like Aggregates. We analyzed the morphology of rPrP aggregates formed upon incubation with D44 or D67 using TEM. An interesting feature when DNA is bound by the rPrP is that DNA induces aggregation of the full-

dx.doi.org/10.1021/bi300440e | Biochemistry 2012, 51, 5402−5413

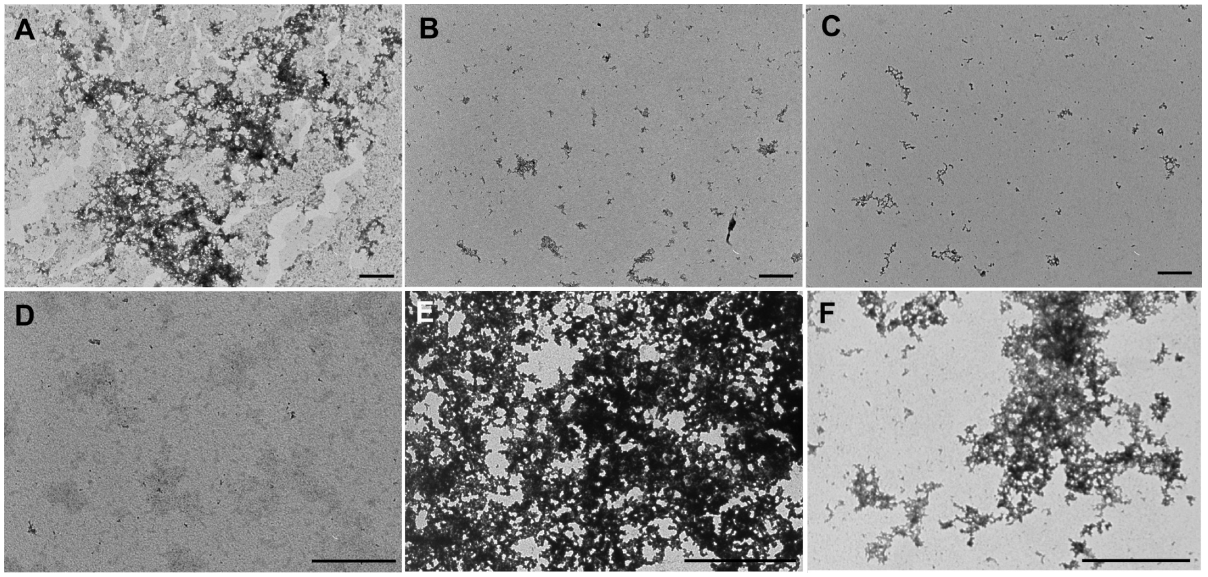

Figure 5. Morphology of rPrP23−231 and Sha109−149 in the presence of D44 and D67 sequences, as observed by transmission electron microscopy: (A) ShaPrP109−149 at 10 μM, (B) 1:1 ShaPrP:D67 molar ratio, (C) 1:1 ShaPrP:D44 molar ratio; (D) free rPrP23−231 at 5 μM, (E) 1:1 rPrP−D67 complex, and (F) 1:1 rPrP−D44 complex. Scale bars are 20 μm.

length sequence but prevents aggregation of the rPrP hydrophobic domains.[11] This feature is observed for other rPrP ligands, as is the case of the hydrophobic probe bis-ANS that also binds both rPrP and PrP peptides.[39] We investigated the morphology of the different complexes of rPrP23−231 and ShaPrP109−149 (a prion protein hydrophobic peptide, comprising residues 109−149) formed when interacting with the D44 and D67 sequences. For ShaPrP109−149, the Syrian hamster prion peptide, we observed that the level of aggregate formation (Figure 5A) was significantly reduced in the presence of either D67 or D44 (Figure 5B,C) in comparison with that of the aggregated peptide (Figure 5A). In contrast, for rPrP23−231 (Figure 5D), we found that both DNA sequences induced the formation of protein aggregates (Figure 5E,F). However, for the D67 sequence, aggregate formation was more pronounced (Figure 5E). These aggregates do not present amyloid-like characteristics but have a fractal-like pattern.

We further investigated whether the interaction of D44 with the Syrian hamster prion peptide would have specificity for the DNA major or minor grooves.

DNA was preincubated with methyl green (a major groove binder) or distamycin (a minor groove binder),[40,41] and inhibition of peptide aggregation was measured using LS. Methyl green partly reverted the inhibitory effect of the DNA on peptide aggregation (Figure S7 of the Supporting Information), indicating that the DNA−ShaPrP109−149 interaction occurs mainly due to contacts through the major groove of the DNA molecule. This result is in agreement with the CD data from the interaction of rPrP23−231 with DNA (Figure 2) because, in general, groove binders lead to the hypochromism of the ∼250 and 275 nm DNA CD bands.[38]

Differential Toxicity Associated with Distinct rPrP−DNA Complexes in Cultured Neuroblastoma Cells. We measured MTT reduction by neuroblastoma cells (N2a) in culture to determine if the rPrP−DNA complexes would lead to cellular dysfunction. We have previously shown that rPrP, when bound to a component of the total RNA extracted from this same cell line, is toxic to N2a cells in culture.[22] However, the specific RNA sequence(s) responsible for this effect is still unknown. To verify whether the toxicity observed was particular to each complex, the complexes were tested in N2a cells.

Interestingly, our results demonstrate that the rPrP−D67 complex caused major cellular dysfunction, verified by a smaller MTT reduction in this case (Figure 6), and that this effect was dose-dependent (Figure 6B). The rPrPΔ51−90 mutant, in the presence of the evaluated DNA sequences, did not alter cellular function (Figure 6A). rPrP was also toxic to N2a cells upon interaction with all control oligonucleotides, except D67A and R67 (Figure S8 of the Supporting Information). The fact that the R67 sequence did not lead to cellular dysfunction is in agreement with our previous work,[22] where only the RNA extract from the N2a cells induced rPrP toxicity and no synthetic RNA sequence (as is the case for R67) led to significant cell dysfunction or death. The complexes with D67 and D67s caused evident cell dysfunction, indicating the role of these GC-rich sequences in rPrP-mediated cellular toxicity.

Viability assays with LIVE/DEAD kits confirmed the MTT reduction data and revealed the toxicity of rPrP23−231 when complexed with the D44 and D67 oligonucleotides, compared to free samples (Figure 7 and Figure S9 of the Supporting Information). Free rPrP23−231 does not affect cell viability, as previously shown.[22] Treatment with Hoechst (Figure 7, fourth column) suggested that the rPrP−D67 complex leads to N2a cell death through apoptosis because these cells presented pyknotic nuclei, as observed by condensed chromatin followed by DNA fragmentation (Figure 7, fourth column). To interpret the mechanism of cell death, we evaluated if incubation with the PrP−NA complexes would induce activation of the caspase-3/7 complex (Figure 8). After incubation for 72 h, only the rPrP−D67A complex induced significant caspase activation (Figure 8). This complex did not affect cell viability, as seen by the MTT reduction assay (Figure S8 of the Supporting Information). We asked whether the most toxic complexes activated caspases before the 72 h point. We then evaluated caspase release with shorter exposure periods (incubation for 24 and 48 h) (Figure 8, black and gray bars). It was possible to see, after incubation for 24 and 48 h, that other rPrP−DNA

dx.doi.org/10.1021/bi300440e | *Biochemistry* 2012, 51, 5402−5413

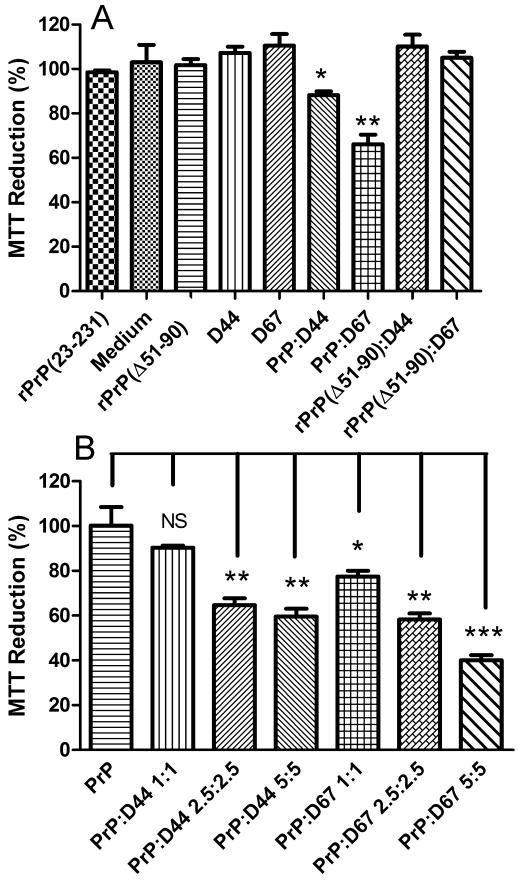

Figure 6. Cellular dysfunction assay for rPrP23−231 and rPrPΔ51−90 in the presence of DNA sequences. (A) Both rPrP constructs (20 μM) were incubated at a 1:1 molar ratio with either D44 or D67, further diluted in the vehicle, and added at a final concentration of 5 μM to each well containing an N2a monolayer. (B) Dose response for rPrP−DNA cytotoxic complexes in N2a cells. rPrP−DNA complexes (rPrP−D44 and rPrP−D67) were incubated at a 1:1 molar ratio, further diluted in the vehicle, and then added at final concentrations of 1, 2.5, or 5 μM to each well containing an N2a monolayer. For panels A and B, MTT reduction was evaluated as described in Experimental Procedures. Data are expressed as the percentage of MTT reduction relative to the free rPrP at the same final concentration. Error bars represent standard deviations of at least three independent measurements, each in triplicate. *P < 0.05; **P < 0.01; ***P < 0.001. NS, nonsignificant.

complexes induced caspase release. There was no direct correlation between toxicity and caspase activation, as the most toxic rPrP−D67, rPrP−D67s, and rPrP−D44 complexes (see Figure S8 of the Supporting Information) did not induce similar levels of caspase-3/7 release at the same incubation interval (Figure 8). We still need to confirm if primary necrosis or fast acting apoptosis is occurring in each case.

We further evaluated if the complexes would impact other cell lines (non-neuronal). We evaluated MTT reduction and performed the LIVE/DEAD assay in HK2 cells (human kidney 2) and found that all complexes are nontoxic to this cell line (Figure S10 of the Supporting Information). Because these types of cells express low PrP^C levels, one might propose that the toxic effects mediated by the rPrP−DNA complexes are dependent on the presence of PrP^C in the extracellular membrane.

DISCUSSION

Although it is common knowledge that the prion protein is responsible for prion diseases, a growing body of evidence indicates the existence of other molecules that chaperone prion misfolding into the scrapie PrP.[11,14,15,25] Among these chaperones are nucleic acids.[13,14] PrP binds nucleic acids, both in vitro and ex vivo,[13,14,22,42] but the effects of such an interaction are still unclear. A recent work suggested the possibility that PrP is not the sole agent of TSEs, as elimination of infectious particles in rat septal cells did not stop production of prions.[43] This result supports the notion that nucleic acids might participate in the pathogenesis of prion diseases. In addition, the participation of RNA molecules in prion physiopathology is also supported by a study indicating that two anti-prion compounds interact with the ribosome in an RNA-dependent manner and inhibit RNA-mediated ribosomal protein folding activity.[44] It was recently shown that a transmembrane form of PrP^C binds Argonaute proteins.[45] This interaction modulates the metabolism of miRNA, probably through binding to nucleic acids.[45]

Herein, we investigate if distinct DNA sequences lead to different aggregations and whether they differently impact the biophysical properties of PrP. We show that the interaction of PrP with two nonrelated DNA sequences, and their respective control sequences, leads to different structures that result in distinct cell toxicity profiles.

We investigated the effects of the interaction of recombinant murine PrP with two nucleic acid sequences previously described as binding to rPrP.[11,36] We observed that the interaction with each of these two sequences led to unique structures. The binding between rPrP and D67, which is a GC-rich sequence (~67% GC content), led to a higher level of aggregation of rPrP (Figure 1), compared to the results observed for binding with D44. However, because the D67A oligonucleotide (28.5% GC content) induced a similar rPrP aggregation, compared to the original D67 sequence, we believe this result is not solely due to differences in GC content but to differences in the sizes of the oligonucleotides (Figure S1 of the Supporting Information). An evaluation of the Stern−Volmer constants (K_{sv}) for rPrP bound to the D67 or D44 sequence (Figure 3 and Table S2 of the Supporting Information) supported the notion that the size of the oligonucleotide is directly related to aggregation propensity. However, while all D44 sequences yielded similar K_{sv} values, interaction with the D67 oligonucleotide resulted in less protection of the Trp residues in comparison to D67A and D67s (Figure 3). Seven of the eight rPrP tryptophan residues are located in the N-terminal flexible domain, and the dissimilar calculated K_{sv} between the D67 sequences might be a result of conformational changes in the N-terminal region, which are dictated by both the DNA structure and the binding site on rPrP.

The rPrP−D44 complex acquired higher thermal stability, with a $T_{1/2}$ ~10 °C higher than that of free rPrP or the rPrP−D67 complex (Figure 4). This higher stability, together with the observation that D44 induces less aggregation of rPrP (Figure 1), may account for the observed differences in cytotoxicity (Figures 6 and 7 and Figure S8 of the Supporting Information).

The rPrP−D67 complex was found to reduce the viability of neuroblastoma cells in culture to a greater degree than the rPrP−D44 complex (Figures 6 and 7 and Figures S8 and S9 of the Supporting Information). To evaluate if this effect was related to only the size of the oligonucleotide (a 21-mer × a 18-

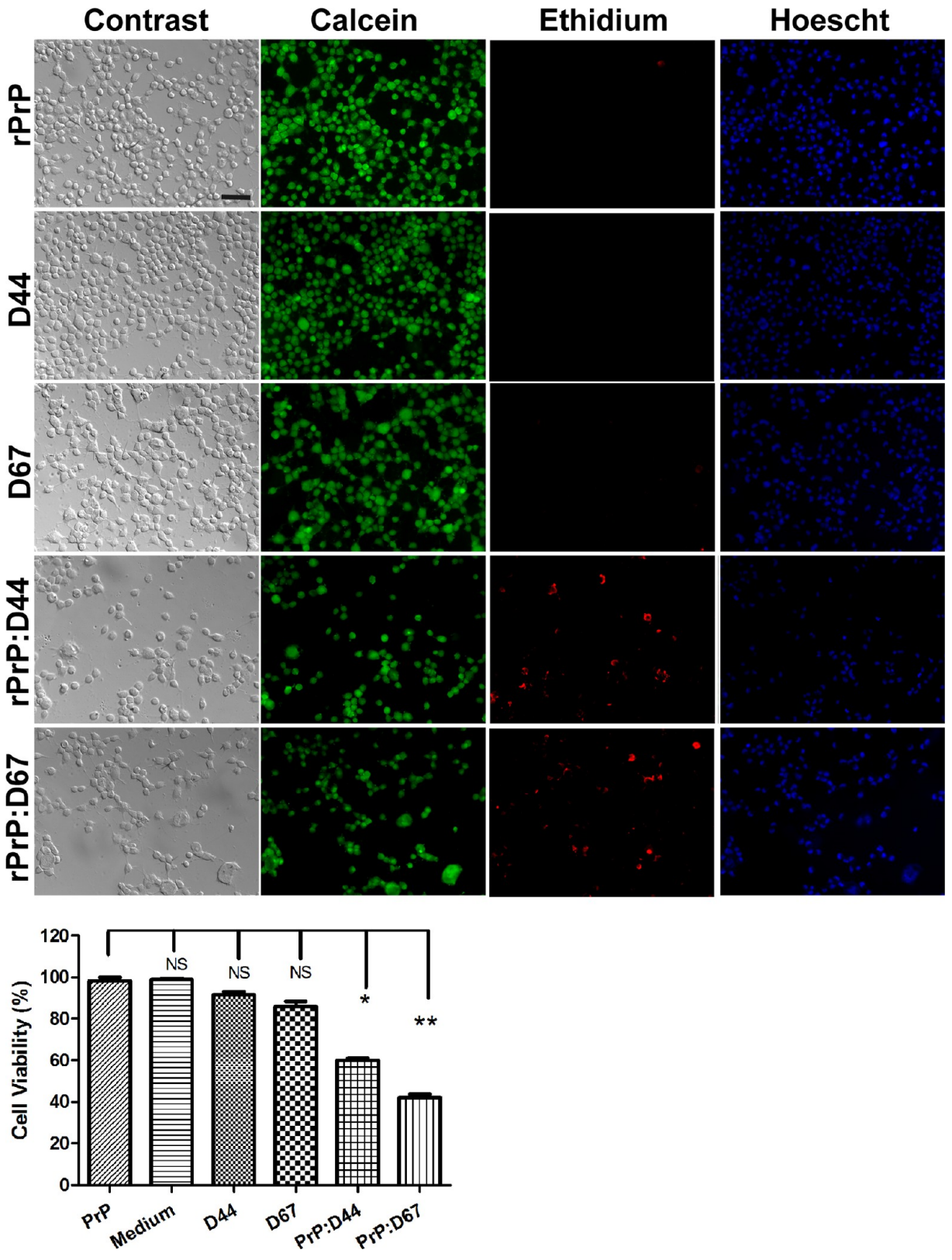

Figure 7. Toxicity of rPrP–DNA complexes, as evaluated by LIVE/DEAD assays. rPrP at 20 μM was incubated at a 1:1 molar ratio with D44 or D67. The assay was performed as described in Experimental Procedures. In the top panel, vertical columns indicate the phase contrast image, calcein emission, ethidium, and Hoechst-33342 fluorescence emission. Horizontal columns show different samples. The scale bar is 50 μm. The bottom panel shows the statistics of the viability assay presented in the top panel. Quantification was performed using five isolated fields for each condition and shows the mean value ± SD. *P < 0.05; **P < 0.01. NS, nonsignificant.

mer sequence), we investigated the impact of the rPrP complexes with the control oligonucleotides in the N2a cell line (Figure S8 of the Supporting Information). We found that the D67s sequence (same size and GC content as D67), when

dx.doi.org/10.1021/bi300440e | *Biochemistry* 2012, 51, 5402–5413

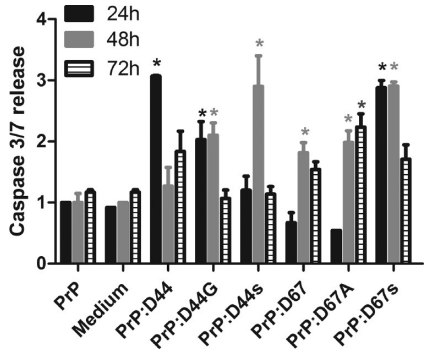

Figure 8. Kinetic evaluation of release of caspase-3/7 by N2a cells in the presence of the rPrP−NA complexes. The samples were incubated with N2a cells at a density of 5×10^3 cells/well for 24, 48, or 72 h at 37 °C with 5% CO_2. Either free rPrP or the rPrP−NA complexes (1:1 molar ratio, 5 μM final concentration) were added to each well. The caspase release assay was performed as described in the technical manual from the ApoTox-Glo Triplex assay (Promega Corp., Madison, WI). The data were normalized in relation to the control (free rPrP) at each specified incubation time (24, 48, or 72 h). *P < 0.05.

bound to rPrP, induced a similar level of cell dysfunction, compared to the D67 oligonucleotide. This effect was not due only to the GC content because the complex with the D44G sequence (~78% GC content) was not as toxic as the ones with the D67 and D67s sequences (Figure S8 of the Supporting Information).

Evaluation of the caspase release induced by the rPrP−NA complexes did not further characterize the cell death mechanism (Figure 8). There was no direct correlation of caspase activation and complex cytotoxicity (Figures 6 and 7 and Figures S8 and S9 of the Supporting Information). This possible controversy might be explained by the fact that the kinetics of cell death mediated by the rPrP−DNA complexes differs among the different oligonucleotides employed and that both primary necrosis or fast-acting apoptosis might be occurring in each case.

Interestingly, the number of cells was reduced in the presence of the complexes (in relation to free rPrP and free DNA), and the morphology of the cells also changed (Figure 7). The N2a cells when incubated with the rPrP−DNA complexes (D44 and D67) did not acquire a neuron-like profile, as happened with the untreated cells or those that were incubated with free rPrP or free DNA after 72 h. The complexes induced a round morphology in the N2a cells, and almost no neurite outgrowth was observed along the incubation time (72 h). This evidence indicates that the rPrP−DNA complexes are indeed affecting cell signaling, which is revealed by altered cellular morphology and differentiation.

The mechanism through which the rPrP−D67 complex mediates toxicity to N2a cells in culture is not yet known. We are currently investigating if these complexes enter the cells and possibly recruit other NA-binding proteins. Because the rPrP−NA complexes did not impact a non-neuronal cell line, it appears that these complexes depend on GPI-anchored PrP^C to mediate their toxic effects in the extracellular milieu (Figure S1 of the Supporting Information). This question is also currently being studied.

It has been suggested that rPrP has two DNA-binding sites, one in the α-helical, C-terminal region and the other in the flexible N-terminus.[36] The interaction between murine rPrP and heparin that takes place at acidic pHs indicates that rPrP has two heparin-binding sites.[46]

Nonspecific DNA binding occurs mainly through the electrostatic and van der Waals interactions of several amino acid residues with the phosphate and deoxyribose groups and is also affected by the nucleic acid's conformation.[47] The amino acids Arg, Lys, and His play an important role in electrostatic interactions. The full-length PrP is highly basic (pI 9.0) and, in murines, contains 11 Arg residues, of which eight are in the C-terminal domain and might mediate nonspecific rPrP−DNA interactions. On the other hand, specific DNA binding takes place mainly through hydrogen bonding between amino acid side chains and the nucleic acid bases. Arg plays a major role in this case because it can make two hydrogen bonds with guanine, thus increasing the interaction specificity.[47] The dsD67 sequence (14 guanine bases) contains ~50% more G content than the dsD44 sequence (8 guanine bases). Therefore, a tighter interaction with the former sequence is expected.

Nuclear magnetic resonance spectra demonstrated that Arg136 of the Syrian hamster PrP is involved in the interaction with the D44 sequence.[36] Histidine residues play an important role in the interaction of PrP with heparin, a glycosaminoglycan that also leads to rPrP biophysical changes.[46]

The CD and FTIR data showed changes in rPrP structure upon DNA binding (Figure 2 and Table 1). After binding equilibrium had been reached, no significant differences in rPrP secondary structure were observed between D67 and D44 binding. However, the LS data indicated a persistent aggregation of the rPrP−D67 complex after equilibrium had been reached (Figure S2 of the Supporting Information). It has been proposed that the exclusion of water molecules due to DNA binding might also affect rPrP misfolding.[48] The rPrPΔ51−90 mutant did not aggregate and was not toxic to cells when incubated with either oligonucleotide (Figure S3 of the Supporting Information and Figure 6A), indicating the role of the amino-terminal region of rPrP in mediating these events. Although in our assays recombinant PrPs alone or the aggregated ShaPrP peptide is nontoxic to cells in culture, the PrP106−126 domain induced toxicity in cultured cells and in vivo systems[49,50] even in the absence of ligands, such as nucleic acids. Evaluating the same system in the presence of oligonucleotides would be worthwhile.

The structure of a protein can be altered by specific or unspecific DNA binding. For most DNA-binding proteins, a combination of specific and unspecific interactions has been found.[51,52] Interestingly, nonspecific interactions of nucleic acids with other proteins that aggregate in the CNS, besides the PrP, have been reported.[16,17,53] A recent study has shown that intact amyloid fibrils of recombinant PrP are highly toxic to cells in culture.[7] This result indicates that different aggregates formed by rPrP under different conditions (in the presence or absence of ligands) might result in a toxic profile similar to that of cellular systems.

Thus, it has been hypothesized that many neurodegenerative diseases occur partly due to an aberrant interaction of the disease-related protein with nucleic acids.[16] In an interesting article, it has been shown that the interaction of short dsDNAs with a bacterial protein domain led to amyloid spheroids and fibers.[54] This result indicates that DNA binding by a bacterial protein promotes amyloidogenesis in a fashion similar to that described for the mammalian prion protein, suggesting a common mechanism for DNA-induced protein aggregation.

Interestingly, prion-like protein aggregates may also be implicated in the normal physiology of the organism. It was recently shown that viral infections induce the formation of MAVS (mitochondrial antiviral signaling) protein aggregates and that those aggregates are indeed active in presenting a prion-like behavior because they form self-conversing fiber-like structures.[55] In this case, it was evident that the prion-like aggregates (generated by the presence of viral RNA) were able to restrict virus replication, displaying, in fact, a gain of function in relation to the nonaggregated MAVS.[55] Moreover, functional prion-like aggregates were also described for the RNA-binding protein CPEB.[56] A self-perpetuating prion-like form was shown to efficiently stimulate the translation of CPEB-regulated mRNA.[56]

These results indicate that NAs might be involved in several pathways leading to nonfunctional or functional amyloid formation, i.e., in physiological or pathological processes.

Circulating DNAs have also been shown to be reliable markers for some human diseases and are detected in the plasma of healthy individuals.[57,58] Prion diseases usually occur in the elderly, in whom the level of cell-free circulating DNA has been found to be at its highest.[59] Thus, PrP−DNA encounters may be more common in this age range.

We show here for the first time that rPrP−DNA interactions lead to aggregated species that, depending on the DNA sequence tested, are toxic to cells in culture. Thus, we suggest that although sequence specificity might not be apparent, there are particular nucleic acid patterns governing PrP recognition, such as oligonucleotide size, GC content, and nucleic acid structure. Further studies that reveal the three-dimensional structure of both PrP−DNA complexes will help in understanding the structural and cellular effects observed in our study. This information may shed light on the still mysterious pathology of the prion protein.

■ ASSOCIATED CONTENT

Supporting Information

Table S2 and Figures S1−S10. This material is available free of charge via the Internet at http://pubs.acs.org.

■ AUTHOR INFORMATION

Corresponding Author

*Universidade Federal do Rio de Janeiro, Faculdade de Farmacia, Av. Carlos Chagas Filho 373, CCS, Bloco B Subsolo Sala 17, Rio de Janeiro, Brazil. Phone: 55 21 22609192, ext. 210. E-mail: yraima@pharma.ufrj.br.

Author Contributions

B.M. and T.A.M. contributed equally to this work.

Funding

This work was supported by grants from Conselho Nacional de Desenvolvimento Científico e Tecnológico (CNPq), the Instituto Nacional de Ciência e Tecnologia de Biologia Estrutural e Bioimagem (INBEB), Coordenação de Aperfeiçoamento de Pessoal de Nível Superior (CAPES), and Fundação de Amparo à Pesquisa do Estado do Rio de Janeiro (FAPERJ) of Brazil.

Notes

The authors declare no competing financial interest.

■ ACKNOWLEDGMENTS

We thank Melissa dos Santos do Nascimento, Ícaro Marques, and Natália do Carmo Ferreira for help in protein purification, Prof. Luís Maurício T. R. Lima for helpful suggestions, Prof. Hernán Terenzi (UFSC) for providing us with the distamycin and methyl green probes, and Dr. Flavio A. Lara for assistance with microscopy.

■ REFERENCES

(1) Prusiner, S. B. (1998) Prions. *Proc. Natl. Acad. Sci. U.S.A. 95*, 13363−13383.

(2) Aguzzi, A., and Polymenidou, M. (2004) Mammalian prion biology: One century of evolving concepts. *Cell 116*, 313−327.

(3) Caughey, B. W., Dong, A., Bhat, K. S., Ernst, D., Hayes, S. F., and Caughey, W. S. (1991) Secondary structure analysis of the scrapie-associated protein PrP 27−30 in water by infrared spectroscopy. *Biochemistry 30*, 7672−7680.

(4) Pan, K. M., Baldwin, M., Nguyen, J., Gasset, M., Serban, A., Groth, D., Mehlhorn, I., Huang, Z., Fletterick, R. J., Cohen, F. E., and Prusiner, S. B. (1993) Conversion of α-helices into β-sheets features in the formation of the scrapie prion proteins. *Proc. Natl. Acad. Sci. U.S.A. 90*, 10962−10966.

(5) Kocisko, D. A., Come, J. H., Priola, S. A., Chesebro, B., Raymond, G. J., Lansbury, P. T., and Caughey, B. (1994) Cell-free formation of protease-resistant prion protein. *Nature 370*, 471−474.

(6) Saborio, G. P., Permanne, B., and Soto, C. (2001) Sensitive detection of pathological prion protein by cyclic amplification of protein misfolding. *Nature 411*, 810−813.

(7) Lee, Y. J., Savtchenko, R., Ostapchenko, V. G., Makarava, N., and Baskakov, I. V. (2011) Molecular structure of amyloid fibrils controls the relationship between fibrillar size and toxicity. *PLoS One 6*, e20244.

(8) Legname, G., Baskakov, I. V., Nguyen, H. O., Riesner, D., Cohen, F. E., DeArmond, S. J., and Prusiner, S. B. (2004) Synthetic mammalian prions. *Science 305*, 673−676.

(9) Caughey, B., and Raymond, G. J. (1993) Sulfated polyanion inhibition of scrapie-associated PrP accumulation in cultured cells. *J. Virol. 67*, 643−650.

(10) DebBurman, S. K., Raymond, G. J., Caughey, B., and Lindquist, S. (1997) Chaperone-supervised conversion of prion protein to its protease-resistant form. *Proc. Natl. Acad. Sci. U.S.A. 94*, 13938−13943.

(11) Cordeiro, Y., Machado, F., Juliano, L., Juliano, M. A., Brentani, R. R., Foguel, D., and Silva, J. L. (2001) DNA converts cellular prion protein into the β-sheet conformation and inhibits prion peptide aggregation. *J. Biol. Chem. 276*, 49400−49409.

(12) Wong, C., Xiong, L. W., Horiuchi, M., Raymond, L., Wehrly, K., Chesebro, B., and Caughey, B. (2001) Sulfated glycans and elevated temperature stimulate PrP(Sc)-dependent cell-free formation of protease-resistant prion protein. *EMBO J. 20*, 377−386.

(13) Deleault, N. R., Geoghegan, J. C., Nishina, K., Kascsak, R., Williamson, R. A., and Supattapone, S. (2005) Protease-resistant prion protein amplification reconstituted with partially purified substrates and synthetic polyanions. *J. Biol. Chem. 280*, 26873−26879.

(14) Silva, J. L., Lima, L. M. T. R., Foguel, D., and Cordeiro, Y. (2008) Intriguing nucleic-acid-binding features of mammalian prion protein. *Trends Biochem. Sci. 33*, 132−140.

(15) Silva, J. L., Gomes, M. P. B., Vieira, T. C. G., and Cordeiro, Y. (2010) PrP interactions with nucleic acids and glycosaminoglycans in function and disease. *Front. Biosci. 15*, 132−150.

(16) Jiménez, J. S. (2010) Protein-DNA interaction at the origin of neurological diseases: A hypothesis. *J. Alzheimer's Dis. 22*, 375−391.

(17) Liu, C., and Zhang, Y. (2011) Nucleic acid-mediated protein aggregation and assembly. *Adv. Protein Chem. Struct. Biol. 84*, 1−40.

(18) Karpuj, M. V., Gelibter-Niv, S., Tiran, A., Rambold, A., Tatzelt, J., Nunziante, M., and Schatzl, H. M. (2011) Conditional modulation of membrane protein expression in cultured cells mediated by prion protein recognition of short phosphorothioate oligodeoxynucleotides. *J. Biol. Chem. 286*, 6911−6917.

(19) Kocisko, D. A., Vaillant, A., Lee, K. S., Arnold, K. M., Bertholet, N., Race, R. E., Olsen, E. A., Juteau, J. M., and Caughey, B. (2006) Potent antiscrapie activities of degenerate phosphorothioate oligonucleotides. *Antimicrob. Agents Chemother. 50*, 1034−1044.

(20) Nandi, P. K., Leclerc, E., Nicole, J. C., and Takahashi, M. (2002) DNA-induced partial unfolding of prion protein leads to its polymerisation to amyloid. *J. Mol. Biol. 322*, 153−161.
(21) Deleault, N. R., Lucassen, R. W., and Supattapone, S. (2003) RNA molecules stimulate prion protein conversion. *Nature 425*, 717−720.
(22) Gomes, M. P. B., Millen, T. A., Ferreira, P. S., Cunha-e-Silva, N. L., Vieira, T. C., Almeida, M. S., Silva, J. L., and Cordeiro, Y. (2008) Prion protein complexed to N2a cellular RNAs through its N-terminal domain forms aggregates and is toxic to murine neuroblastoma cells. *J. Biol. Chem. 283*, 19616−19625.
(23) Nandi, P. K., and Nicole, J. C. (2004) Nucleic acid and prion protein interaction produces spherical amyloids which can function in vivo as coats of spongiform encephalopathy agent. *J. Mol. Biol. 344*, 827−837.
(24) Strom, A., Wang, G. S., Picketts, D. J., Reimer, R., Stuke, A. W., and Scott, F. W. (2011) Cellular prion protein localizes to the nucleus of endocrine and neuronal cells and interacts with structural chromatin components. *Eur. J. Cell Biol. 90*, 414−419.
(25) Deleault, N. R., Harris, B. T., Rees, J. R., and Supattapone, S. (2007) Formation of native prions from minimal components in vitro. *Proc. Natl. Acad. Sci. U.S.A. 104*, 9741−9746.
(26) Wang, F., Wang, X., Yuan, C. G., and Ma, J. (2010) Generating a prion with bacterially expressed recombinant prion protein. *Science 327*, 1132−1135.
(27) Karpuj, M. V., Giles, K., Gelibter-Niv, S., Scott, M. R., Lingappa, V. R., Szoka, F. C., Peretz, D., Denetclaw, W., and Prusiner, S. B. (2007) Phosphorothioate Oligonucleotides Reduce PrPSc Levels and Prion Infectivity in Cultured Cells. *Mol. Med. 13*, 190−198.
(28) Rhie, A., Kirby, L., Sayer, N., Wellesley, R., Disterer, P., Sylvester, I., Gill, A., Hope, J., James, W., and Tahiri-Alaoui, A. (2003) Characterization of 2′-fluoro-RNA aptamers that bind preferentially to disease-associated conformations of prion protein and inhibit conversion. *J. Biol. Chem. 278*, 39697−39705.
(29) Takemura, K., Wang, P., Vorberg, I., Surewicz, W., Priola, S. A., Kanthasamy, A., Pottathil, R., Chen, S. G., and Sreevatsan, S. (2006) DNA aptamers that bind to PrP(C) and not PrP(Sc) show sequence and structure specificity. *Exp. Biol. Med. 231*, 204−214.
(30) Liu, M. L., Wen, J. J., Xu, X. F., and Zhao, D. M. (2011) Neurotoxic Effect of the Complex of the Ovine Prion Protein (OvPrP(C)) and RNA on the Cultured Rat Cortical Neurons. *Neurochem. Res. 36*, 1863−1869.
(31) Cordeiro, Y., Kraineva, J., Gomes, M. P. B., Lopes, M. H., Martins, V. R., Lima, L. M. T. R., Foguel, D., Winter, R., and Silva, J. L. (2005) The amino-terminal PrP domain is crucial to modulate prion misfolding and aggregation. *Biophys. J. 89*, 2667−2676.
(32) Lima, L. M. T. R., and Silva, J. L. (2004) Positive contribution of hydration on DNA binding by E2c protein from papillomavirus. *J. Biol. Chem. 279*, 47968−47974.
(33) Macedo, B., Kaschula, C. H., Hunter, R., Chaves, J. A., van der Merwe, J. D., Silva, J. L., Egan, T. J., and Cordeiro, Y. (2010) Synthesis and anti-prion activity evaluation of aminoquinoline analogues. *Eur. J. Med. Chem. 45*, 5468−5473.
(34) Byler, D. M., and Susi, H. (1986) Examination of the secondary structure of proteins by deconvolved FTIR spectra. *Biopolymers 25*, 469−487.
(35) Cordeiro, Y., Kraineva, J., Ravindra, R., Lima, L. M. T. R., Gomes, M. P. B., Foguel, D., Winter, R., and Silva, J. L. (2004) Hydration and packing effects on prion folding and β-sheet conversion. High pressure spectroscopy and pressure perturbation calorimetry studies. *J. Biol. Chem. 279*, 32354−32359.
(36) Lima, L. M. T. R., Cordeiro, Y., Tinoco, L. W., Marques, A. F., Oliveira, C. L., Sampath, S., Kodali, R., Choi, G., Foguel, D., Torriani, I., Caughey, B., and Silva, J. L. (2006) Structural insights into the interaction between prion protein and nucleic acid. *Biochemistry 45*, 9180−9187.
(37) Marques, A. F., Cordeiro, Y., Silva, J. L., and Lima, L. M. T. R. (2009) Enhanced prion protein stability coupled to DNA recognition and milieu acidification. *Biophys. Chem. 141*, 135−139.
(38) Uma Maheswaria, P., and Palaniandavar, M. (2004) DNA binding and cleavage properties of certain tetrammine ruthenium(II) complexes of modified 1,10-phenanthrolines: Effect of hydrogen-bonding on DNA-binding affinity. *J. Inorg. Biochem. 98*, 219−230.
(39) Cordeiro, Y., Lima, L. M., Gomes, M. P., Foguel, D., and Silva, J. L. (2004) Modulation of prion protein oligomerization, aggregation, and β-sheet conversion by 4,4′-dianilino-1,1′-binaphthyl-5,5′-sulfonate (bis-ANS). *J. Biol. Chem. 279*, 5346−5352.
(40) Van Dyke, M. W., Hertzberg, R. P., and Dervan, P. B. (1982) Map of distamycin, netropsin, and actinomycin binding sites on heterogeneous DNA: DNA cleavage-inhibition patterns with methidiumpropyl-EDTA·Fe(II). *Proc. Natl. Acad. Sci. U.S.A. 79*, 5470−5474.
(41) Kim, S. K., and Nordén, B. (1993) Methyl green. A DNA major-groove binding drug. *FEBS Lett. 315*, 61−64.
(42) Beaudoin, S., Vanderperre, B., Grenier, C., Tremblay, I., Leduc, F., and Roucou, X. (2009) A large ribonucleoprotein particle induced by cytoplasmic PrP shares striking similarities with the chromatoid body, an RNA granule predicted to function in posttranscriptional gene regulation. *Biochim. Biophys. Acta 1793*, 335−345.
(43) Miyazawa, K., Kipkorir, T., Tittman, S., and Manuelidis, L. (2012) Continuous production of prions after infectious particles are eliminated: Implications for Alzheimer's disease. *PLoS One 7* (4), e35471.
(44) Tribouillard-Tanvier, D., Dos Reis, S., Gug, F., Voisset, C., Béringue, V., Sabate, R., Kikovska, E., Talarek, N., Bach, S., Huang, C., Desban, N., Saupe, S. J., Supattapone, S., Thuret, J. Y., Chédin, S., Vilette, D., Galons, H., Sanyal, S., and Blondel, M. (2008) Protein folding activity of ribosomal RNA is a selective target of two unrelated antiprion drugs. *PLoS One 3*, e2174.
(45) Gibbings, D., Leblanc, P., Jay, F., Pontier, D., Michel, F., Schwab, Y., Alais, S., Lagrange, T., and Voinnet, O. (2012) Human prion protein binds Argonaute and promotes accumulation of microRNA effector complexes. *Nat. Struct. Mol. Biol. 19*, 517−524.
(46) Vieira, T. C., Reynaldo, D. P., Gomes, M. P. B., Almeida, M. S., Cordeiro, Y., and Silva, J. L. (2011) Heparin Binding by Murine Recombinant Prion Protein Leads to Transient Aggregation and Formation of RNA-Resistant Species. *J. Am. Chem. Soc. 133*, 334−344.
(47) Luscombe, N. M., Laskowski, R. A., and Thornton, J. M. (2001) Amino acid-base interactions: A three-dimensional analysis of protein-DNA interactions at an atomic level. *Nucleic Acids Res. 29*, 2860−2874.
(48) Silva, J. L., Vieira, T. C., Gomes, M. P. B., Ano Bom, A. P., Lima, L. M. T. R., Freitas, M. S., Ishimaru, D., Cordeiro, Y., and Foguel, D. (2010) Ligand binding and hydration in protein misfolding: Insights from studies of prion and p53 tumor suppressor proteins. *Acc. Chem. Res. 43*, 271−279.
(49) Ettaiche, M., Pichot, R., Vincent, J. P., and Chabry, J. (2000) In vivo cytotoxicity of the prion protein fragment 106−126. *J. Biol. Chem. 275*, 36487−36490.
(50) Gong, J., Jellali, A., Forster, V., Mutterer, J., Dubus, E., Altrock, W. D., Sahel, J. A., Rendon, A., and Picaud, S. (2007) The Toxicity of the PrP106−126 Prion Peptide on Cultured Photoreceptors Correlates with the Prion Protein Distribution in the Mammalian and Human Retina. *Am. J. Pathol. 170*, 1314−1324.
(51) Ohlendorf, D. H., and Matthew, J. B. (1985) Electrostatics and flexibility in protein-DNA interactions. *Adv. Biophys. 20*, 137−151.
(52) Pabo, C. O., and Nekludova, L. (2000) Geometric analysis and comparison of protein-DNA interfaces: Why is there no simple code for recognition? *J. Mol. Biol. 301*, 597−624.
(53) Parekh-Olmedo, H., Wang, J., Gusella, J. F., and Kmiec, E. B. (2004) Modified single-stranded oligonucleotides inhibit aggregate formation and toxicity induced by expanded polyglutamine. *J. Mol. Neurosci. 24*, 257−267.
(54) Giraldo, R. (2007) Defined DNA sequences promote the assembly of a bacterial protein into distinct amyloid nanostructures. *Proc. Natl. Acad. Sci. U.S.A. 104*, 17388−17393.
(55) Hou, F., Sun, L., Zheng, H., Skaug, B., Jiang, Q. X., and Chen, Z. J. (2011) MAVS forms functional prion-like aggregates to activate and propagate antiviral innate immune response. *Cell 146*, 448−461.

(56) Si, K., Lindquist, S., and Kandel, E. R. (2003) A neuronal isoform of the aplysia CPEB has prion-like properties. *Cell 115*, 879–891.
(57) Suzuki, N., Kamataki, A., Yamaki, J., and Homma, Y. (2008) Characterization of circulating DNA in healthy human plasma. *Clin. Chim. Acta 387*, 55–58.
(58) Yoon, K. A., Park, S., Lee, S. H., Kim, J. H., and Lee, J. S. (2009) Comparison of circulating plasma DNA levels between lung cancer patients and healthy controls. *J. Mol. Diagn. 11*, 182–185.
(59) Jylhävä, J., Kotipelto, T., Raitala, A., Jylhä, M., Hervonen, A., and Hurme, M. (2011) Aging is associated with quantitative and qualitative changes in circulating cell-free DNA: The Vitality 90+ study. *Mech. Ageing Dev. 132*, 20–26.

NOTE ADDED AFTER ASAP PUBLICATION

This paper was published to the Web with a mistake in the figure 6 caption on June 25, 2012. This was fixed in the version published on June 28, 2012.